Polymer Composites

WILEY | spe INSPIRING PLASTICS PROFESSIONALS

RESEARCH ARTICLE

Mode-II Fracture and Residual Flexural Strength of MWCNT Modified E-Glass/Epoxy Laminates

Coşkun Yildiz[1] | Fatih Daricik[2]

[1]Department of Mechanical Engineering, Akdeniz University, Antalya, Turkey | [2]Department of Mechanical Engineering, Alanya Alaaddin Keykubat University, Antalya, Turkey

Correspondence: Fatih Daricik (fatih.daricik@alanya.edu.tr)

Received: 27 January 2025 | **Revised:** 22 March 2025 | **Accepted:** 22 July 2025

Keywords: GFRP composite | interlaminar fracture mechanics | mode-II crack propagation | multiwalled carbon nanotubes

ABSTRACT

In this study, three types of carboxyl-functionalized multi-walled carbon nanotubes (MWCNTs) were used to modify the mode-II interlaminar fracture characteristics and residual bending resistance of E-glass/epoxy composite laminates. The MWCNTs with different weight ratios were added into the matrix material, and the mode-II interlaminar fracture toughness and the fracture propagation were investigated in accordance with the relevant ASTM standards. Fractured surfaces were inspected with SEM micrographs to justify the effects of MWCNTs on the mode-II fracture of the laminate. The MWCNTs increased the adhesion of constituents in the laminates and obstructed the propagation of delamination. The MWCNTs enhanced mode-II interlaminar fracture toughness and bending stiffness of the E-glass/epoxy laminates. The short-thin MWCNTs at 0.3 wt% increased mode-II interlaminar fracture resistance of the laminate by about 2 times. The effects of long-thin and long-thick MWCNTs are quite low.

1 | Introduction

Fiber reinforced composite (FRC) laminates are often used in the form of plates in industrial applications. Composite laminates are subjected to out-of-plane loads that can lead to bending under service conditions. This bending may cause the coalescence of micro-voids, interlayer cracks to merge, and propagate through the matrix-rich interlayer zone. Invisible cracks that develop between the layers in the composite material can result in delamination of the layers and a loss of structural integrity. For this reason, many studies have been conducted over the last 30 years on the mode-II fracture characteristics of laminated composite materials. The formation and propagation of delamination in laminated composite materials depend on the mechanical properties of the matrix material and the strength of the matrix-fiber interface, rather than the continuous fibers [1, 2]. This is because the matrix materials that hold the fibers together and bond the layers possess low mechanical strength and are often brittle. To mitigate these disadvantages of matrix materials, nano or micro-sized particles can be added to improve their mechanical properties.

Many researchers used silica, fly ash, nano clay, nano rubber, etc. to increase the mechanical strength of the polymer matrix [3–12]. Some researchers have also succeeded in improving the mechanical properties of epoxy by adding carbon nanotube particles [13–16]. Improving the mechanical properties of the matrix material by using particles with high mechanical properties suggests that the same effect can be achieved in laminated composite materials. Recent investigations proved that the elastic properties and mechanical strength of laminated composite materials produced by adding particles are better than those of the neat material [7, 17–21].

When the effect of nanoparticle additives on the interlaminar fracture characteristics of the laminates is examined, it has been observed that the particles prevent crack development by filling their inner spaces with matrix material and forming a bridge

Summary

- Adding MWCNTs into E-glass/epoxy laminates increases G_{IIc} up to 77%.
- MWCNT additives provide hot-spot induced crazing of the polymer.
- Crazing, fiber bridging, and pull-out are the micro-mechanisms increasing G_{IIc}.
- Adding MWCNTs also increases residual flexural strength of delaminated E-glass/epoxy laminates.

between the fractured surfaces, increasing the adhesion at the fiber/matrix interface by adhering to the reinforcement fibers and causing the fibers to peel. The improvements are obvious and severally reported in literature, especially for mode-I interlaminar fracture of the laminates [22–28].

The use of nanoparticles to enhance interlaminar strength in laminated composite materials has become an intriguing research topic over the past two decades. Wang et al. claimed that modifying the interlayer of CFRP laminates with short aramid fibers significantly improves mode-II toughness and flexural properties [29]. Le et al. used vertically aligned carbon nanotubes to investigate how the nanotubes affect interlaminar crack propagation. They concluded that the cusps of vertically aligned carbon nanotubes cause brittle nature and unstable crack propagation in CFRP produced with prepregs [30]. Saikia et al. reported that the hydroxyl functionalized MWCNTs added in weight ratio up to 0.2% can increase mode-II interlaminar fracture toughness up to 18% while a higher ratio causes reduction [31].

The literature survey put forth that the investigations on interlaminar fracture of the laminated composites focused on carbon fiber/epoxy laminates. There is a lack of knowledge about the acts of MWCNTs on the mode-II fracture behavior of the E-glass/epoxy laminates. However, the effect of the MWCNTs' size and weight ratio is not frankly reported in the literature. The residual flexural strength of the delaminated E-glass/epoxy laminates has never been reported before. In this research, the mode-II fracture characteristics of MWCNTs modified E-glass/epoxy laminates were investigated. The dimensional difference of the MWCNTs and their weight ratio are selected as research parameters, so the optimum MWCNT has been selected to enhance mode-II interlaminar resistance of the laminate. However, since the laminate continues to be used until detecting the crack, the residual flexural strength of the laminates was also investigated. The fractured surface morphology of both unmodified and nanoparticle-modified materials was inspected to explain the micro-mechanisms laying behind the change of interlaminar fracture characteristics.

2 | Experimental

2.1 | Materials

The constituents of the laminate are unidirectional E-glass fabric and DGBA laminating epoxy resin. The unidirectional E-glass fabric consists of glass filaments that are attached to each other using stitching yarns with a density of 10 stitches/in. and have an areal weight of 300 g/cm^2. As matrix material, Hexion brand diglycidyl bisphenol A (DGBA) type MGS L160 epoxy and H160 hardener were used. To improve interlaminar properties of the laminates, we added three types of MWCNTs differing by outer diameter, inner diameter, length, and specific area into resin (Table 1). We bought carboxylic acid (–COOH) functionalized MWCNTs from supplier US Research Nanomaterials Inc. The MWCNTs were weighed out accurately and added to the epoxy at weight rates of 0.1%, 0.3%, 0.7%, and 0.9%.

TABLE 1 | Specifications of the COOH-MWCNTs.

Specification	Unit	CNT 1	CNT 2	CNT 3
Outer diameter	Nm	10–20	30–50	10–20
Inner diameter	Nm	5–10	5–12	5–10
Length	Mm	10–30	10–20	0.50–2
Purity	%	> 95	> 95	> 95
Specific area	m^2/g	> 200	> 60	> 200
True density	g/cm^3	≈2.1	≈2.1	≈2.1
Bulk density	g/cm^3	0.22	0.22	0.22

TABLE 2 | Physical and mechanical properties of the unmodified E-glass/epoxy composite laminate [22].

Properties	Symbol	Value (Unit)	Test method
Fiber volume fraction	V_f	47.25 (%)	ASTM D3171
Density	ρ_c	1.75 (g/cm^3)	ASTM D792
Longitudinal elastic modulus	E_{11}	33.28 (GPa)	
Transverse elastic modulus	E_{22}	8.84 (GPa)	
Longitudinal strength	S_1	612.07 (MPa)	ASTM D3039
Transverse strength	S_2	88.61 (MPa)	
Major Poisson's ratio	ν_{12}	0.30	
In-plane shear modulus	G_{12}	4.59 (GPa)	ASTM D3518
In-plane shear strength	τ_{max}	48.13 (MPa)	

2.2 | Manufacturing of E Glass/Epoxy Composite Laminates

The E-glass/epoxy laminates were manufactured with a vacuum bagging method to avoid filtration influence of the fibers for MWCNTs. Some physical and mechanical properties of

the E-glass/epoxy laminate were known from the previous investigation [22] and presented in Table 2. In order to produce nanoparticle modified composite laminates, the MWCNTs were added into the epoxy resin within the determined weight ratios and mixed with a magnetic stirrer. The resulting nanoparticle and epoxy mixture was sonicated with an ultrasonic bath for 6 h. In this way, a homogeneous distribution of particles that are likely to clump in the epoxy is ensured. Ultrasonication is a frequently used method to ensure the homogeneous distribution of nanoparticles in a liquid. In this method, ultrasonic sound waves propagate by diluting the molecular structure in the environment and force the molecular structure forming the environment to vibrate. At this time, the clumped nanoparticles are separated, and at the same time, it is easier for the diluted epoxy to penetrate into the nanoparticles with a porous structure. If the ultrasonication process is applied for too long or with high power, the carbon nanotube particles may be damaged. During the sonication process, the temperature of the water in the bath was controlled, and the required safe temperature value (> 45°C) for the epoxy was followed.

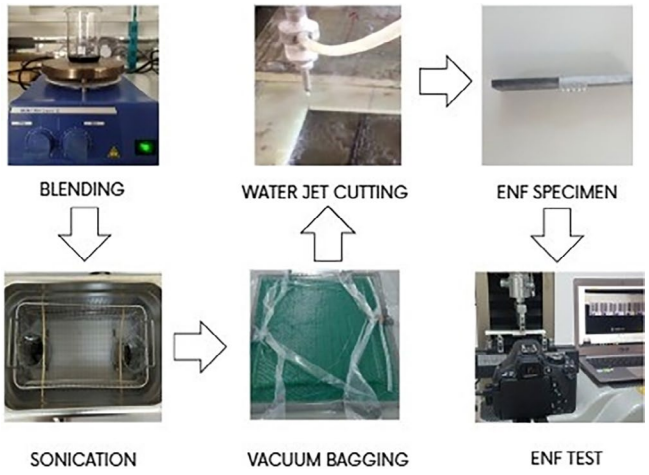

FIGURE 1 | Manufacturing of MWCNT modified laminate.

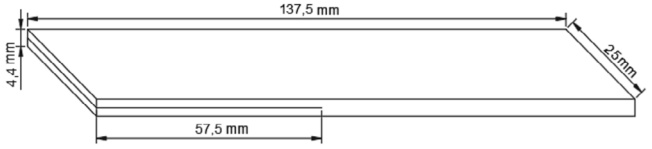

FIGURE 2 | ENF test specimen with artificial delamination.

The unmodified and MWCNT modified E-glass/epoxy composite laminates with a stacking sequence of $[0_{16}]$ were then manufactured by the vacuum bagging method. The vacuumed layers were kept under 1 atm pressure for 24 h and then subjected to a post-cure process in a 40°C oven for 12 h. The thickness of the laminates was 4.4 mm. We located a mold release agent-coated

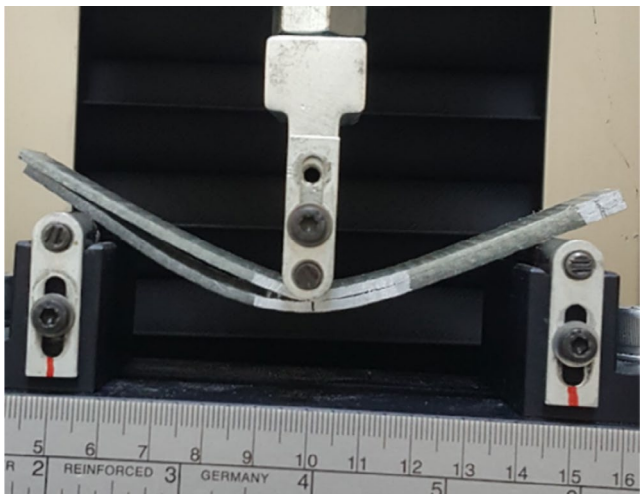

FIGURE 4 | 3-point bending test of delaminated ENF laminates.

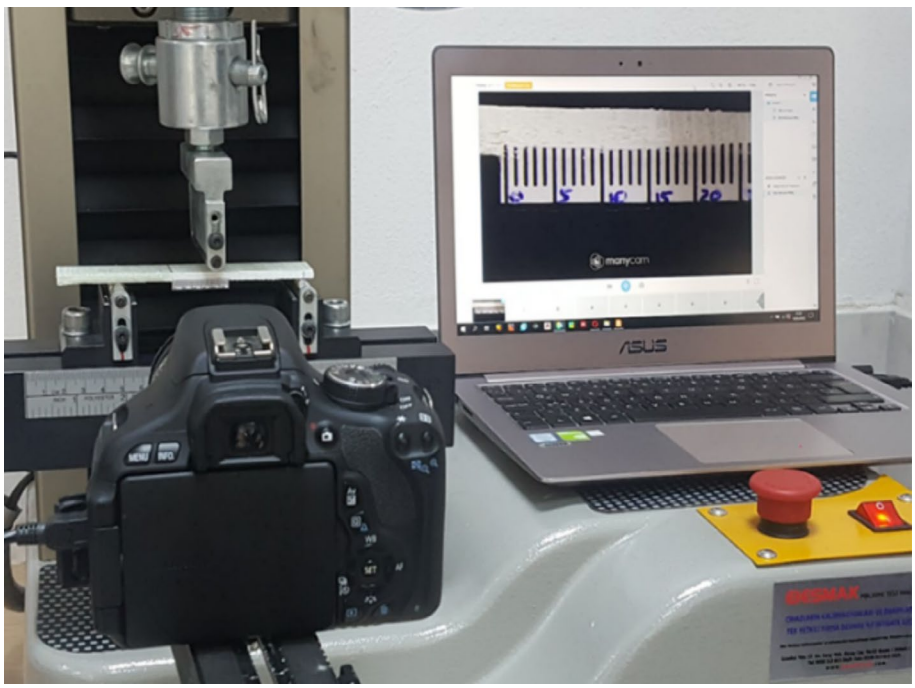

FIGURE 3 | Experimental setup for the mode-II interlaminar fracture test of the E-glass/epoxy laminate.

12 μm thick PET film in the middle interface to get an artificial precrack. The manufacturing of the laminates with artificial precrack, the specimen preparation, and the mode-II fracture test were shown in Figure 1.

2.3 | Mechanical Testing

Displacement controlled mode-II fracture toughness of the laminates was determined according to the ASTM D7905-14 method [32]. The end notched flexure (ENF) specimens were cut in dimensions ($L \times w \times h$) of 137.5 × 25 × 4.4 mm from the unmodified and MWCNT modified laminates (Figure 2). CNC water jet was used for the cutting process. The longer sides of ENF specimens were painted white with water-based correction fluid, to make the crack tip more visible. The displacement control for the test was satisfied with a three-point bending test apparatus having 5 mm dia loading and support rollers. The support span of the apparatus was set as 100 mm. The ENF specimens were located to have a 25 mm distance from the load application points to the artificial crack tip (a_0). Before the test, a paper ruler was pasted on the painted side by aligning the lower sublaminate. Cracks were followed on the painted surface.

The specimens were deflected with a crosshead displacement rate of 0.75 mm/min by a single column tabletop universal testing machine having a class 0.5–10 kN load cell. The deflection and reaction force values were recorded to draw the P-δ curve. The crack tip was monitored during the test with a Canon EOS 650D brand camera having 10X magnification. Thus, the slow and steady crack propagation was observed before catastrophic rupture. The test and the digital camera recording were started concurrently. The duration of the test was also recorded to match the displacement and force reaction data with the advancing crack length. Mode-II fracture toughness tests were repeated six times for each specimen type (Figure 3).

The mode-II strain energy release rate (G_{II}) can be calculated from the following beam theory expression using the measured compliance C:

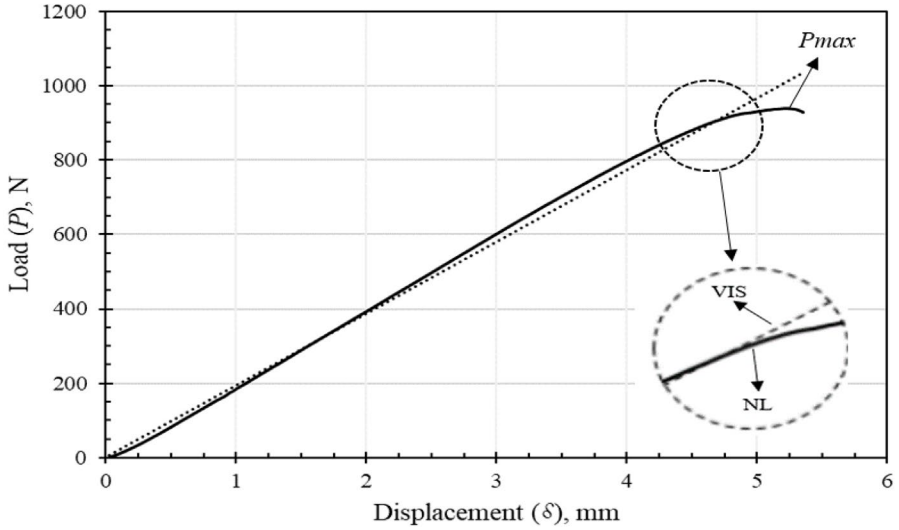

(a)

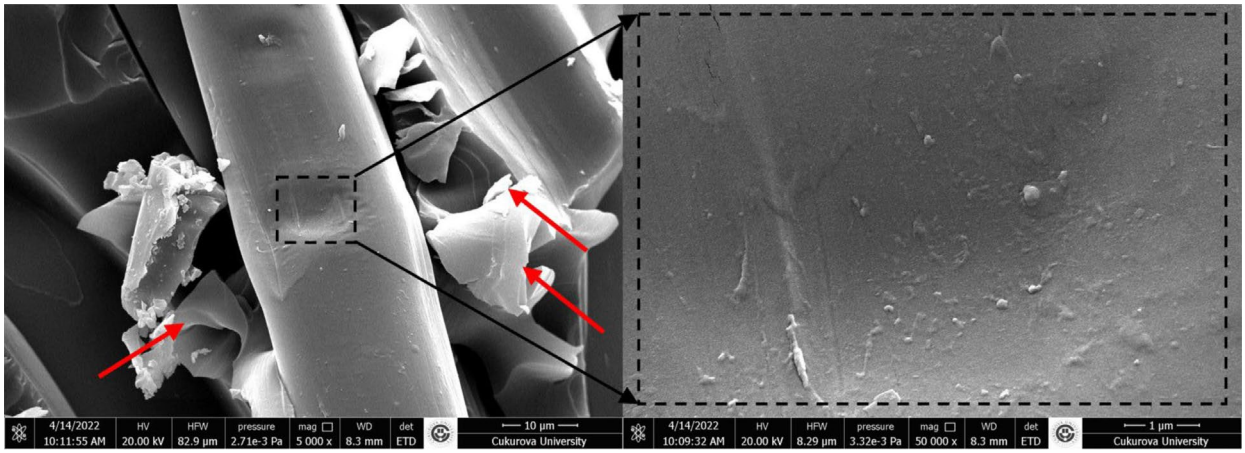

(b)

FIGURE 5 | (a) P-δ curve and (b) fractured surface of the unmodified E-glass/epoxy laminate.

$$G_{II} = \frac{9a^2P^2\left(C - C_{SH}\right)}{4bL^3\left[1 + 1,5\left(\frac{a}{L}\right)^3\right]} \quad (1)$$

here C_{SH} is a compliance correction factor resulting from the calculated interlayer shear deformation. G_{13} is used to calculate the C_{SH} value. However, if the G_{13} value is not known, the in-plane shear modulus G_{12} can be used as an equivalent to G_{13} for unidirectional composites [33].

$$C_{SH} = \frac{6L + 3a - l^3/a^2}{20bhG_{13}} \quad (2)$$

The mode-II fracture toughness (G_{IIc}) of the laminated composite material was calculated using the critical load (P_{cr}) and displacement (δ_{cr}) required to propagate the delamination crack. Critical load and displacement were found by observing (Visual Observation—VIS) according to ASTM D7905-14 method and by determining the point where the *P*-δ graph diverged from linearity (*NL* point).

2.3.1 | Bending Tests of Delaminated Laminates

The mode-II fracture tests represented that although the delamination crack advanced at mid-interface, the upper and lower sublaminates were not fractured. With the presence of intact layers, it was thought that the material could withstand a little more bending load. In order to determine the residual bending strength of the delaminated specimens, the three-point bending tests were performed (Figure 4). The bending tests were carried out according to ASTM D790-15 standard [34].

The support span (2L) was adjusted as 100 mm. The displacement rate was determined according to Equation 3 and was calculated as 3.79 mm/min. The test was terminated when one of the upper or lower sublaminates was fractured. The load and displacement data were processed to calculate the flexural strength (Equation 4).

$$R = ZL^2 / 6d \quad (3)$$

$$\sigma_f = 3PL / 2bd2 \quad (4)$$

2.3.2 | Fractography

The fractured surfaces were inspected via SEM. The MWCNTs and their interfaces with the matrix material and the fiber were investigated to identify the effect of the interaction on mode-II fracture toughness. SEM specimens were cut with a rotating diamond saw in dimensions of 4×2 mm, cleaned in an ultrasonic bath, and coated with Au-Pd via sputter, respectively. The FEI brand Quanta 650 Field Emission SEM scanning electron microscope was used to take SEM images. The specimens were charged with 20 kV, and the surfaces were monitored with magnification up to 50,000×.

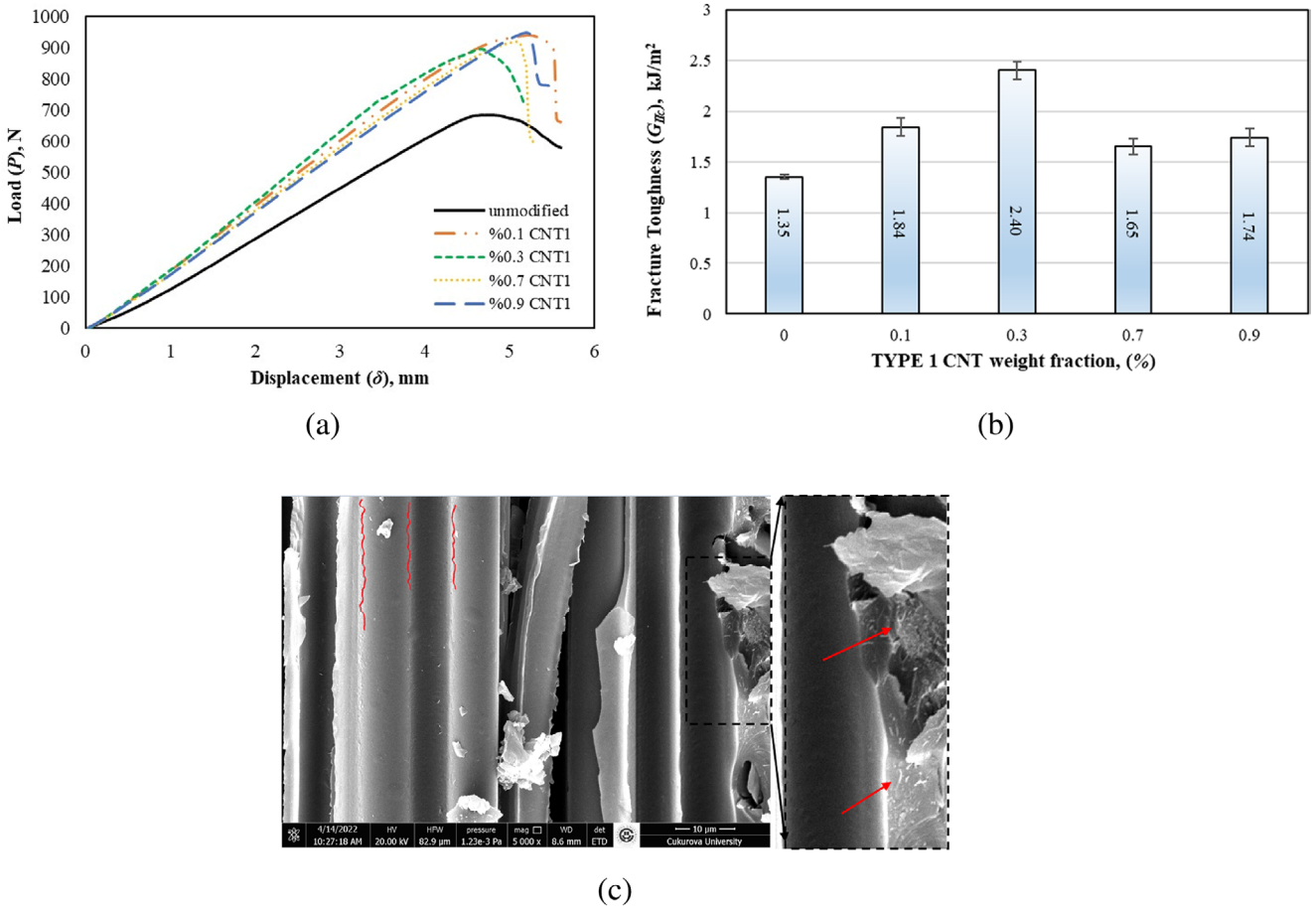

FIGURE 6 | (a) *P*-δ curves, (b) G_{IIc} values, and (c) fractured surface micrographs of TYPE 1 CNTs modified laminates.

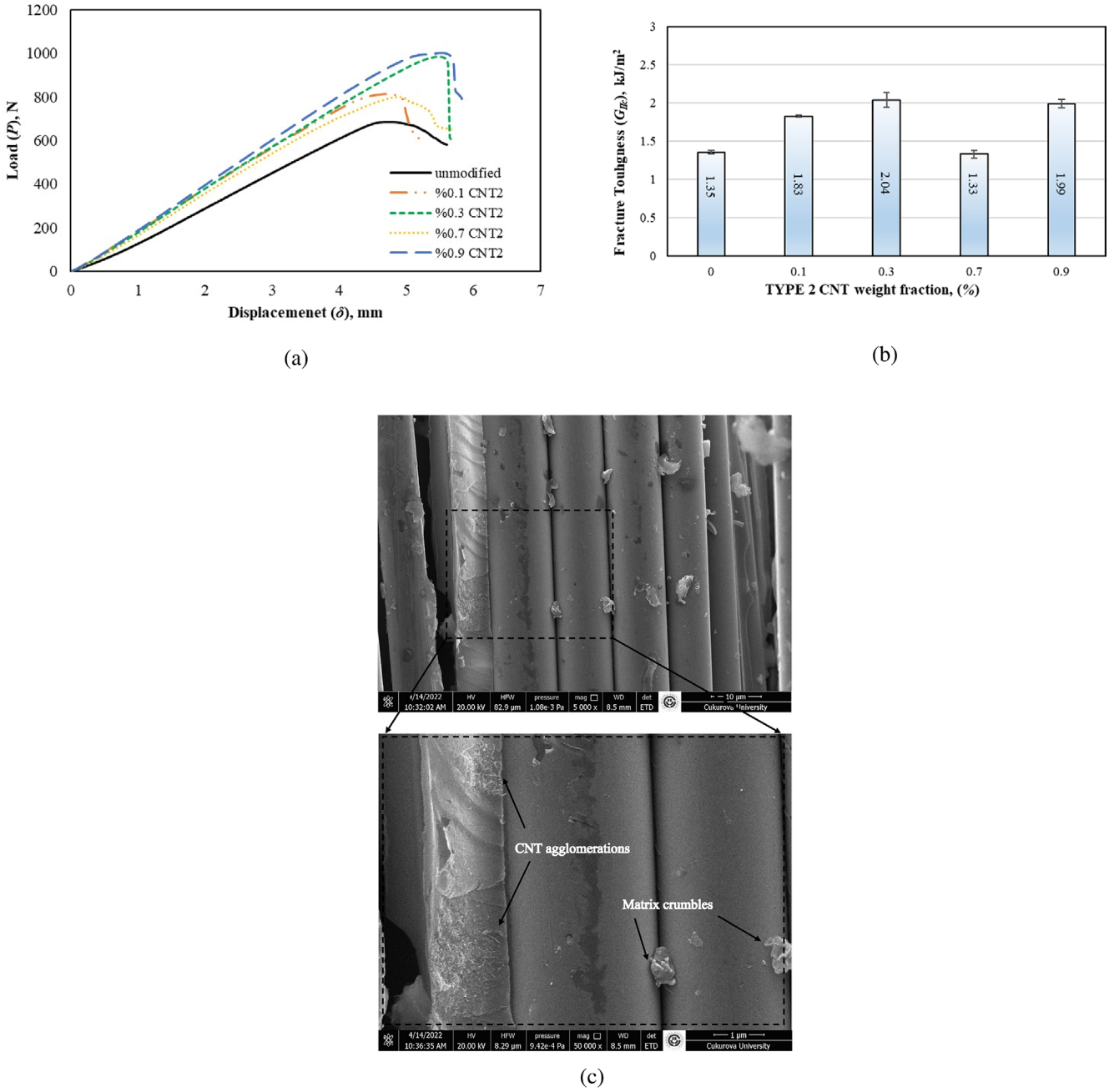

FIGURE 7 | (a) P-δ curves, (b) G_{IIc} values, (c) fractured surface micrographs of TYPE 2 CNTs modified laminates.

3 | Results and Discussion

3.1 | Mode-II Fracture Tests

A characteristic P-δ curve of an unmodified ENF specimen was presented in Figure 4a. The point where the P-δ curve deviates from linearity was determined as the *NL* point, and the corresponding P-δ values were saved as the critical (P_{cr}-δ_{cr}). The values were used to calculate the G_{IIc}. The point at which the crack initiation was first seen via monitoring was determined as the VIS point, and the critical P-δ values can also be determined with visual inspection. The methods (VIS point, NL point) have been recommended in ASTM D7905-14 for determining P_{cr} and δ_{cr} values are shown in Figure 5a. Although P_{cr} and δ_{cr} obtained by both methods are very close to each other, the P_{cr} value determined according to the *NL* point and its corresponding δ_{cr} value are the more conservative. However, the VIS point was not evident for all specimens, so the P_{cr} and δ_{cr} values obtained with the VIS method were not used to calculate G_{IIc}.

In the linear region of the P-δ curve, the precrack withstood the work done on it. The deviation from linearity was evident for the crack tip advancing. Shortly after, the load response of the specimen reached a maximum (P_{max}) and the rapid crack tip propagation took place. Daricik and Aslan calculated the average C value to be 0.1546 mm/N according to the VIS point and 0.1590 mm/N according to the NL point for the unmodified E-glass/epoxy [22].

It has been observed that in regions where epoxy is abundant, the fractured surfaces do not contain sharp edges or tips but

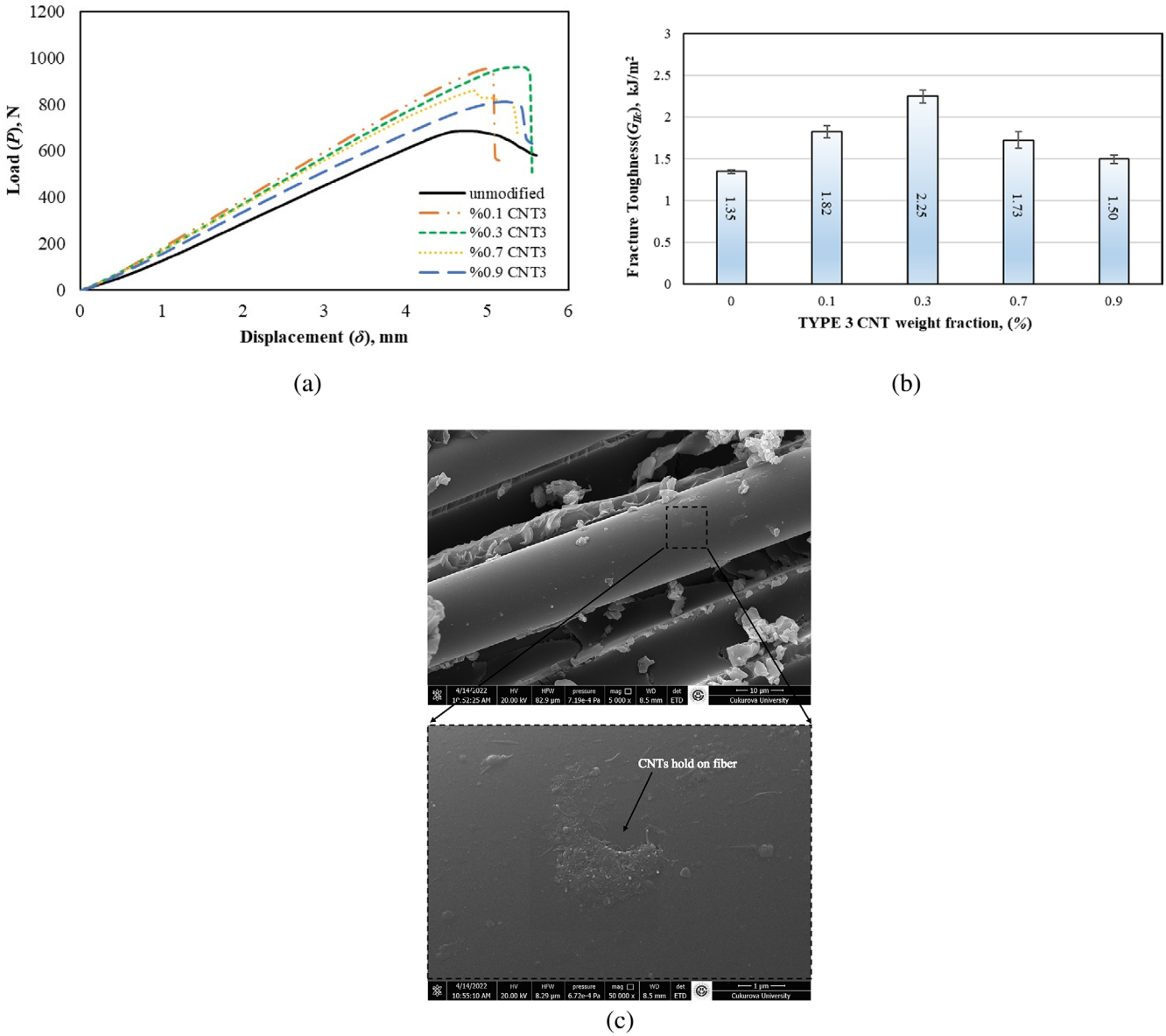

FIGURE 8 | (a) P-δ curves, (b) G_{IIc} values, (c) fractured surface micrographs of TYPE 3 CNTs modified laminates.

consist of non-sharp radius crimps and smooth surfaces called "river lines" (Figure 5b). Some crumbled epoxy particles were also seen. The river lines on the fracture surfaces of the epoxy matrix indicate that the fracture is brittle. Because the fibers were also free of epoxy, it was considered that the adhesion between E-glass fiber/epoxy is poor [2, 35].

P-δ curves of E-glass fiber/epoxy laminates with TYPE 1 CNTs additives were presented in Figure 6a. When the obtained *P-δ* curves were compared, it was understood that the bending stiffness of the material increases with the addition of TYPE 1 CNTs. However, the increase in bending stiffness is not linearly proportional to the CNTs ratio. The laminates containing 0.3% CNT by weight showed the highest resistance to bending load, with a steeper *P-δ* curve than the others.

In the TYPE 1 CNT modified laminates, the highest G_{IIC} value was observed at the rate of 0.3% by weight with an increase of 77.7%. The least increase (22.2%) was seen at the rate of 0.7% by weight (Figure 6b). The reasons for the findings were investigated by examining the fracture surface morphology (Figure 6c). The sides of fiber-induced grooves in TYPE 1 CNT modified laminates are more serrated than those of unmodified specimens. The serrated sides are an indication of the good adhesion of fiber and resin. The resin-rich regions are rougher due to the CNT agglomeration. These random CNT agglomerations are also obstructions for crack propagation.

P-δ curves of the TYPE 2 CNT modified E-glass fiber/epoxy laminates were presented in Figure 7a. The presence of TYPE 2 CNTs increased the bending stiffness of the laminates with respect to the unmodified laminates. E-glass fiber/epoxy composite material containing 0.9% by weight CNT showed the highest resistance to bending load. The G_{IIc} of the TYPE 2 CNTs added laminates is also obviously higher than that of the unmodified one. But the highest improvement of G_{IIc} (51.1%) was obtained with the addition of TYPE 2 CNT in a weight ratio of 0.3% (Figure 7b).

TABLE 3 | P_{max}, δmax, and σmax values for bending tests.

Test samples	Particle ratio by weight (%)	P_{max} (N)	δ_{max} (mm)	σ_{max} (Mpa)	%CV
Neat	0	908.63	21.10	269.22	2.00
TYPE 1 CNT	0.1	1147.66	21.92	352.07	2.84
	0.3	1076.66	23.35	319.01	1.71
	0.7	1016.42	25.16	301.15	2.00
	0.9	1004.73	22.28	297.69	2.88
TYPE 2 CNT	0.1	1065.81	20.00	315.79	4.58
	0.3	1054.12	23.07	312.33	3.60
	0.7	1105.94	26.51	327.68	1.19
	0.9	1047.58	21.26	310.39	2.23
TYPE 3 CNT	0.1	1040.70	21.58	308.35	2.29
	0.3	1115.69	25.57	330.57	1.81
	0.7	1072.74	24.09	317.85	2.81

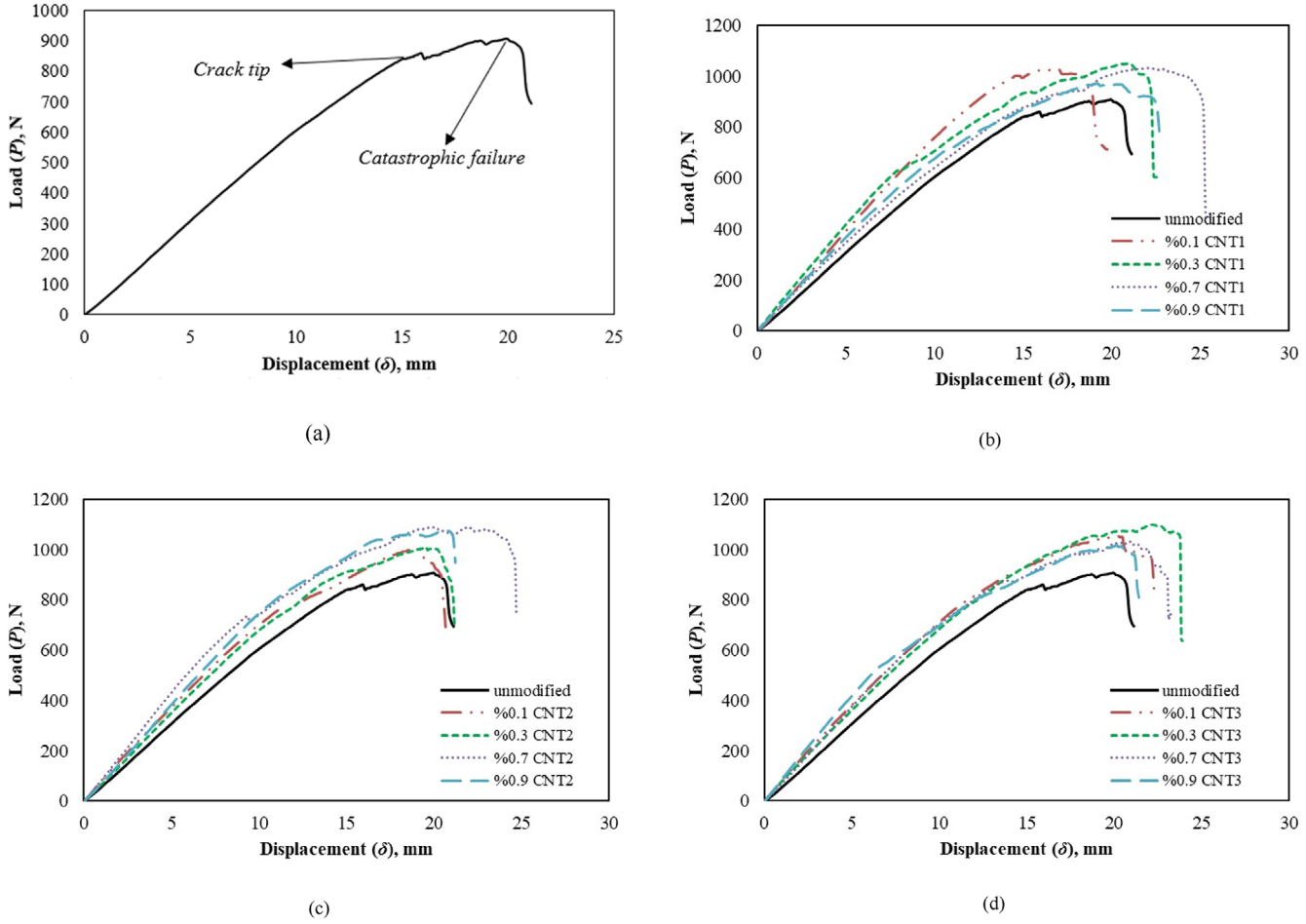

FIGURE 9 | *P-δ* curve of the laminates due to 3-point bending test (a) unmodified laminate, (b) TYPE 1 CNTs modified laminate, (c) TYPE 2 CNTs modified laminate, and (d) TYPE 3 CNTs modified laminate.

In Figure 7c, the scanning electron microscopy of the TYPE 2 CNT modified fractured surfaces was presented. The hold of MWCNTs onto fibers is obvious. The fractured surfaces of the matrix were also rough, including crumbles of epoxy, especially in the vicinity of the fibers. The saw teeth formations took place at the edges of grooves. Fiber grooves formed by the separation of fiber and epoxy showed the sawtooth damage mechanism due to shear stress at the delamination

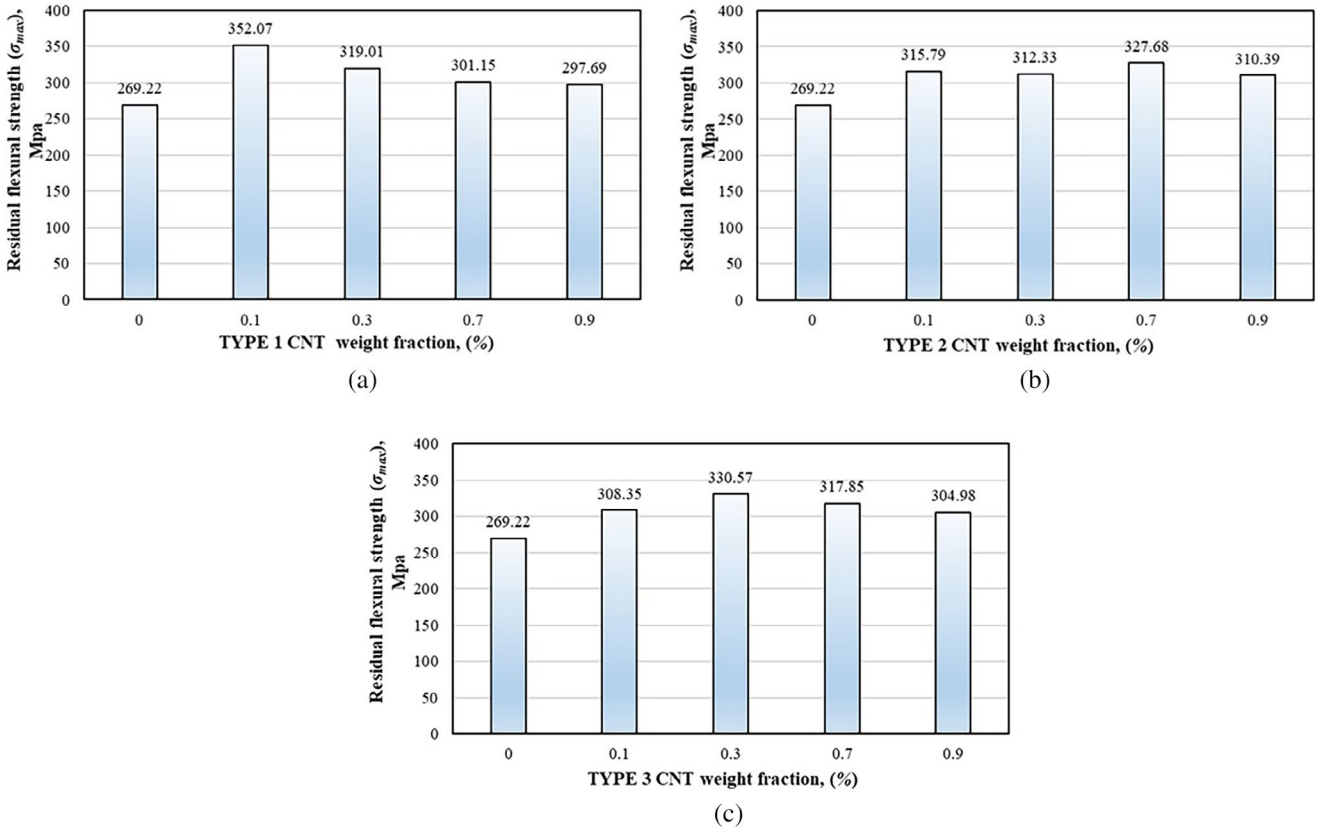

FIGURE 10 | Variation of σ_{max} (a) TYPE 1 CNTs modified laminate, (b) TYPE 2 CNTs modified laminate, and (c) TYPE 3 CNTs modified laminate.

interface, along with fiber/epoxy damage during delamination development [36]. With increased crack propagation, the intensity of sawtooth damage mechanisms, as well as corrugated fiber deposits, increases significantly, and the fracture surface becomes rougher compared to the previous stage (the beginning of crack growth) [37]. As can be seen, saw teeth are the dominant damage mechanism occurring perpendicular to the fiber direction. Saw teeth are one of the most important fractographic features observed in composites and are frequently observed in mode-II and mixed mode-I/II delamination growth due to shear stress [38, 39]. These patterns are brittle matrix microcracks that generally form perpendicular to the maximum principal stress. The roughness of the fracture surface indicates the formation of fiber bridges and, therefore, the presence of carbon nanoparticles. By examining the surface morphology of TYPE 2 CNTs modified laminates, it was seen that the epoxy-surrounded fibers are more abundant than those of the unmodified specimen. Rough surfaces of the groove indicate that the adhesion force between the fiber and matrix in TYPE 2 CNTs modified laminates is quite high.

P-δ curves of TYPE 3 CNT modified laminates were presented in Figure 8a. The addition of TYPE 3 CNTs also supplied an increase in the bending stiffness of the laminates. The laminates with 0.1% TYPE 3 CNT addition by weight showed the highest resistance to bending load. In TYPE 3 CNT modified E-glass fiber/epoxy composite materials, the highest G_{IIc} was observed at the rate of 0.3% by weight with an increase of 66.6%, and the least increase was seen at the rate of 0.9% by weight with an increase of 11.1% (Figure 8b).

The general characteristics of the fracture surface of the TYPE 3 CNTs modified laminates are similar to the fracture surfaces of the TYPE 1 CNTs and TYPE 2 CNTs modified laminates. It was observed that the TYPE 3 CNTs agglomerated and held on the fiber surface (Figure 8c). This may have increased the adhesion strength of the fiber and the matrix material. The matrix material crumbles were also seen on the fractured surfaces of TYPE 3 CNTs modified laminates. The presence of nanoparticles in the matrix effectively suppresses the initiation and propagation of microcracks. The CNTs were also held on the surface of the fiber. Nanoparticles near the fiber matrix region make crack propagation more branched and complex [40].

Separation of the fiber surface from the epoxy creates significant voids, resulting in a large fracture surface area. A significant amount of deformation energy is consumed here, resulting in a significant improvement in fracture toughness values. The presence of nanoparticles thus increases the efficiency of stress transfers between fiber matrix layers, providing evidence for enhanced fiber matrix interface adhesion [41].

3.2 | Residual Flexural Strength of ENF Samples

After mode-II fracture tests were performed, the structural integrity of MWCNT modified E-glass fiber/epoxy laminated composite materials was not completely damaged. The 8th delamination at the interface has progressed, but there is no visible damage to the upper and lower layers with $[0_8]$ alignment. Therefore, it is thought that there is residual flexural strength

in laminated composites even with the progress of delamination. The residual flexural strength (σ_{max}) of the unmodified and modified laminates was given in Table 3 with %CV. The results were highly consistent with the lowest 1.19% coefficient of variation.

The deflection and load response curves of the unmodified and modified laminates due to 3-point bending test were given in Figure 9. Due to the deflection, the delamination at the middle interface progressed a little further. Afterwards, the sample carried some more load and finally suddenly broke with lost of integrity. The upper sublaminate was broken firstly. The same nature of failure was emerged for all of the MWCNTs modified laminates. In the mode II fracture tests, the ENF specimens were deflected in a range of 4 to 5 mm and corresponding reaction force was recorded in the range of 750–1000 N. But we have deflected the specimens up to 20 mm during the flexural tests, since the corresponding reaction forces were still in the range of 750–1000 N.

The residual flexural strength of the unmodified and modified laminates was compared in the column graphs (Figure 10). The significant improvement of MWCNTs on the residual flexural strength of the laminates was obvious. The maximum increase in the residual flexural strength was obtained with a rate of 30.8% and the minimum increase was obtained with a rate of 10.6%.

4 | Conclusions

The effects of MWCNTs with differing dimensions and weight ratios on the mode-II interlaminar fracture resistance and the residual flexural strength of E-glass/epoxy laminates were investigated in this study. Based on the results, we infer that:

- It is possible to increase the G_{IIc} and bending stiffness of E-glass/epoxy laminated composites by adding COOH-MWCNTs in different weight ratios.
- By adding MWCNTs with a weight ratio of 0.3, the G_{IIc} of E-glass/epoxy laminated composites can be increased up to 77%.
- The presence of CNTs provides good adhesion at the fiber–matrix interface, making crack propagation difficult.
- Although the CNT agglomeration was undesirable, the CNT agglomeration made the fractured matrix surfaces rougher, which indicates the increase in fracture toughness.
- The MWCNT also increased the residual flexural strength of the E-glass/epoxy laminates.
- Although the delamination progressed with mode-II fracture and the bending stiffness of the E-glass/epoxy laminates decreased, the laminates retained their bending load carrying capacity.

Author Contributions

Coşkun Yildiz conducted the experimental studies, data analysis, and prepared the original draft of the manuscript. Fatih Daricik supervised the research, contributed to the interpretation of results, and reviewed and edited the manuscript. Both authors approved the final version of the manuscript.

Conflicts of Interest

The authors declare no conflicts of interest.

Data Availability Statement

The data that support the findings of this study are available from the corresponding author upon reasonable request.

References

1. J. Argüelles, A. F. Viña, J. Canteli, and J. Bonhomme, "Fatigue Delamination, Initiation, and Growth, Under Mode I and II of Fracture in a Carbon-Fiber Epoxy Composite," *Polymer Composites* 31, no. 4 (2010): 700–706.

2. V. Mirjalili, R. Ramachandramoorthy, and P. Hubert, "Enhancement of Fracture Toughness of Carbon Fiber Laminated Composites Using Multi Wall Carbon Nanotubes," *Carbon* 79 (2014): 413–423.

3. K. Y. Azeez, S. J. Rhee, D. Park, and D. Hui, "Epoxy Clay Nanocomposites—Processing, Properties and Applications: A Review," *Composites Part B, Engineering* 45 (2013): 308–320.

4. A. O. Fulmali, B. Sen, B. C. Ray, and R. K. Prusty, "Effects of Carbon Nanotube/Polymer Interfacial Bonding on the Long-Term Creep Performance of Nanophased Glass Fiber/Epoxy Composites," *Polymer Composites* 41 (2020): 478–493.

5. A. O. Fulmali, S. K. Ramamoorthy, R. K. Prusty, J. Abraham, S. Thomas, and N. Kalarikkal, eds., *Handbook of Carbon Nanotubes* (Springer International Publishing, 2020), 1–41.

6. Kishore and S. Santra, "Impact Studies in Elastomer, Fly Ash, and Hybrid-Filled Epoxy Composites: Part I-Room Temperature Curing," *Journal of Reinforced Plastics and Composites* 24, no. 9 (2005): 903–922.

7. C. M. Manjunatha, A. C. Taylor, A. J. Kinloch, and S. Sprenger, "The Tensile Fatigue Behaviour of a Silica Nanoparticle-Modified Glass Fibre Reinforced Epoxy Composite," *Composites Science and Technology* 70 (2010): 193–199.

8. S. R. Rama and S. K. Rai, "Mechanical and Fractrographic Studies on Fly Ash-Filled Hydroxyl-Terminated Polyurethane-Toughened Epoxy Composites," *Journal of Composite Materials* 43, no. 26 (2009): 3231–3238.

9. S. R. Rama and S. K. Rai, "Studies on Physicomechanical Properties of Fly Ash-Filled Hydroxyl-Terminated Polyurethane-Toughened Epoxy Composites," *Journal of Reinforced Plastics and Composites* 29, no. 14 (2010): 2099–2104.

10. S. R. Rama and S. K. Rai, "Deformation and Fracture Behavior of Treated Fly Ash-Filled Polycarbonate-Toughened Epoxy Resin Composites," *Journal of Reinforced Plastics and Composites* 5, no. 30 (2011): 389–395.

11. Y. Tang, L. Ye, Z. Zhang, and K. Friedrich, "Interlaminar Fracture Toughness and CAI Strength of Fibre-Reinforced Composites With Nanoparticles—A Review," *Composites Science and Technology* 37 (2013): 26–37.

12. M. F. Uddin and C. Sun, "Strength of Unidirectional Glass/Epoxy Composite With Silica Nanoparticle-Enhanced Matrix," *Composites Science and Technology* 68 (2008): 1637–1643.

13. C. Chen, S. Nesbitt, J. Reiner, R. Vaziri, A. Poursartip, and G. Fernlund, "Cure Path Dependency of Static and Dynamic Mode II Interlaminar Fracture Toughness of Interlayer Toughened Composite Laminates," *Composites Science and Technology* 200 (2020): 108444.

14. F. H. Gojny, M. H. Wichmann, B. Fiedler, and K. Schulte, "Influence of Different Carbon Nanotubes on the Mechanical Properties of Epoxy Matrix Composites—A Comparative Study," *Composites Science and Technology* 65 (2005): 2300–2313.

15. B. S. Hadavand, K. M. Javid, and M. Gharagozlou, "Mechanical Properties of Multi-Walled Carbon Nanotube/Epoxy Polysulfide Nanocomposite," *Materials and Design* 50 (2013): 62–67.

16. H. Ulus, T. Üstün, V. Eskizeybek, Ö. S. Şahin, and A. Avcı, "Boron Nitride-MWCNT/Epoxy Hybrid Nanocomposites: Preparation and Mechanical Properties," *Applied Surface Science* 318 (2014): 37–42.

17. M. Sayer, "Elastic Properties and Buckling Load Evaluation of Ceramic Particles Filled Glass/Epoxy Composites," *Composites Part B: Engineering* 59 (2014): 12–20.

18. M. Y. Shen, T. Y. Chang, T. H. Hsieh, et al., "Mechanical Properties and Tensile Fatigue of Graphene Nanoplatelets Reinforced Polymer Nanocomposites," *Journal of Nanomaterials* 2013 (2013): 1–9.

19. A. Subagia, L. D. Tijing, Y. Kim, C. S. Kim, F. P. Vista, IV, and H. K. Shon, "Mechanical Performance of Multiscale Basalt Fiber–Epoxy Laminates Containing Tourmaline Micro/Nano Particles," *Composites Part B, Engineering* 58 (2014): 611–617.

20. J. Zhang, S. Ju, D. Jiang, and H. X. Peng, "Reducing Dispersity of Mechanical Properties of Carbon Fiber/Epoxy Composites by Introducing Multi-Walled Carbon Nanotubes," *Composites Part B: Engineering* 54 (2013): 371–376.

21. Y. Zhou, M. Hosur, S. Jeelani, and P. K. Mallick, "Fabrication and Characterization of Carbon Fiber Reinforced Clay/Epoxy Composite," *Journal of Materials Science* 42 (2012): 5002–5012.

22. F. Daricik and Z. Aslan, "Effects of Carbon Nanotube Size on the Mode I Interlaminar Fracture Behavior of E-Glass/Epoxy Nanocomposites: Static Loading," *Polymer Composites* 43, no. 8 (2022): 5260–5273.

23. V. Eskizeybek, A. Avci, and A. Gülce, "The Mode I Interlaminar Fracture Toughness of Chemically Carbon Nanotube Grafted Glass Fabric/Epoxy Multi-Scale Composite Structures," *Composites Part A: Applied Science and Manufacturing* 63 (2014): 94–102.

24. Y. Zhu, C. E. Bakis, and J. H. Adair, "Effects of Carbon Nanofiller Functionalization and Distribution on Interlaminar Fracture Toughness of Multi-Scale Reinforced Polymer Composites," *Carbon* 50 (2012): 1316–1331.

25. P. M. Ajayan, L. S. Schadler, C. Giannaris, and A. Rubio, "Single-Walled Carbon Nanotube–Polymer Composites: Strength and Weakness," *Advanced Materials* 12 (2000): 750–753.

26. Y. L. Chen, B. Liu, X. Q. He, Y. Huang, and K. C. Hwang, "Failure Analysis and the Optimal Toughness Design of Carbon Nanotube-Reinforced Composites," *Composites Science and Technology* 70 (2010): 1360–1367.

27. V. Mirjalili and P. Hubert, "Modelling of the Carbon Nanotube Bridging Effect on the Toughening of Polymers and Experimental Verification," *Composites Science and Technology* 70 (2010): 1537–1543.

28. P. Agnihotri, S. Basu, and K. K. Kar, "Effect of Carbon Nanotube Length and Density on the Properties of Carbon Nanotube-Coated Carbon Fiber/Polyester Composites," *Carbon* 49 (2011): 3098–3106.

29. Y. Wang, X. Liu, L. Chen, W. Shen, and L. Zhu, "Simultaneously Improve the modeIIinterlaminar Fracture Toughness, Flexural Properties, and Impact Strength ofCFRPcomposites With Short Aramid Fiber Interlaminar Toughening," *Polymer Composites* 43, no. 11 (2022): 8437–8442.

30. A. T. Le, Q. Govignon, S. Rivallant, and T. Cutard, "Mode I and Mode II Fracture Behavior in Nano-Engineered Long Fiber Reinforced Composites," *Polymer Composites* 44, no. 7 (2023): 4016–4026.

31. P. J. Saikia, M. Kumar, A. Kumar, and N. Muthu, "Experimental Estimation and Numerical Validation of Cohesive Zone Parameters in Hydroxyl Functionalized MWCNTs-Reinforced CFRP Under Pure Mode II Loading," *Polymer Composites* 45, no. 9 (2024): 8236–8250.

32. ASTM D7905M-14, "Standard Test Method for Determination of the Mode-II Interlaminar Fracture Toughness of Unidirectional Fiber-Reinforced Polymer Matrix Composites," 2014.

33. L. A. Carlsson, D. F. Adams, and R. B. Pipes, *Experimental Characterization of Advanced Composite Materials* (CRC Press, 2014).

34. ASTM D790-15, "Standard Test Methods for Flexural Properties of Unreinforced and Reinforced Plastics and Electrical Insulating Materials," 2016.

35. N. A. Siddiqui, R. S. Woo, J. K. Kim, C. C. Leung, and A. Munir, "Mode I Interlaminar Fracture Behavior and Mechanical Properties of CFRPs With Nanoclay-Filled Epoxy Matrix," *Composites Part A: Applied Science and Manufacturing* 38 (2007): 449–460.

36. M. Salamat-Talab, M. M. Shokrieh, and M. Mohaghegh, "On the R-Curve and Cohesive Law of Glass/Epoxy End-Notch Flexure Specimens With 0//θ Interface Fiber Angles," *Polymer Testing* 2021, no. 93 (2021): 106992.

37. R. Mohammadi, M. A. Najafabadi, H. Saghafi, and D. Zarouchas, "Fracture and Fatigue Behavior of Carbon/Epoxy Laminates Modified by Nanofibers," *Composites Part A: Applied Science and Manufacturing* 137 (2020): 106015.

38. J. Bonhomme, A. Argüelles, J. Vina, and I. Vina, "Fractography and Failure Mechanisms in Static Mode I and Mode II Delamination Testing of Unidirectional Carbon Reinforced Composites," *Polymer Testing* 28, no. 6 (2009): 612–617.

39. T. Johannesson, P. Sjöblom, and R. Selden, "The Detailed Structure of Delamination Fracture Surfaces in Graphite/Epoxy Laminates," *Journal of Materials Science* 19 (1984): 1171–1177.

40. V. Prasad, K. Sekar, S. Varghese, and M. A. Joseph, "Enhancing Mode I and Mode II Interlaminar Fracture Toughness of Flax Fibre Reinforced Epoxy Composites With Nano TiO_2," *Composites Part A Applied Science and Manufacturing* 124 (2019): 105505.

41. Y. Tian, H. Zhang, and Z. Zhang, "Influence of Nanoparticles on the Interfacial Properties of Fiber-Reinforced-Epoxy Composites," *Composites Part A: Applied Science and Manufacturing* 98 (2017): 1–8.